

Viscous heating effects in fluids with temperature-dependent viscosity: triggering of secondary flows

By **A. COSTA**^{1,2,3†} AND **G. MACEDONIO**²

¹Osservatorio Vesuviano - INGV, Via Diocleziano 328, Naples, Italy

²Department of Earth Sciences, University of Bologna, Via Zamboni, Bologna, Italy

³Department of Earth Sciences, University of Pisa, Via S. Maria 53, 56126 Pisa, Italy

(Received ?? and in revised form ??)

Viscous heating can play an important role in the dynamics of fluids with strongly temperature-dependent viscosities because of the coupling between the energy and momentum equations. The heat generated by viscous friction produces a local temperature increase near the tube walls with a consequent decrease of the viscosity and a strong stratification in the viscosity profile. The problem of viscous heating in fluids was investigated and reviewed by Costa & Macedonio (2003) because of its important implications in the study of magma flows.

Due to the strong coupling between viscosity and temperature, the temperature rise due to the viscous heating may trigger an instability in the velocity field, which cannot be predicted by a simple isothermal newtonian model. When the viscous heating produces a pronounced peak in the temperature profile near the walls, with a consequent strong increase in the viscosity gradient, a triggering of instabilities and the transition to secondary flows can occur. Recent experimental results (White & Muller 2000) show that

† Present address: Osservatorio Vesuviano - INGV, Via Diocleziano 328, 80124 Naples, Italy.

in the case of a Taylor-Couette flow viscous heating can reduce by an order of magnitude the critical Reynolds number of the system.

In this paper we focus on the thermal and mechanical effects caused by viscous heating. We will show, as in certain regimes, these effects can trigger and sustain a particular class of secondary rotational flows which appear organized in coherent structures similar to roller vortices. This phenomenon can play a very important role in the dynamics of magma flows in conduits and lava flows in channels and, to our knowledge, it is the first time that it has been investigated by a direct numerical simulation.

1. Introduction

In this paper we show that the effects of viscous heating can play an important role in the dynamics of fluids with strongly temperature-dependent viscosities such as silicate melts and polymers. In fact, in these fluids, viscous friction generates a local increase in temperature near the tube walls with consequent viscosity decrease and increase of the flow velocity. This velocity increase produces a further growth of the local temperature. As recently described in Costa & Macedonio (2003), there are some critical values of the parameters that control this process above which this feedback cannot converge. In this case the one-dimensional laminar solution, valid in the limit of an infinitely long pipe, cannot exist even for low Reynolds numbers. In pipes of finite lengths, viscous heating governs the evolution from a Poiseuille regime with a uniform temperature distribution at the conduit inlet, to a plug flow with a hotter boundary layer near the walls downstream (Pearson 1977; Ockendon 1979). When the temperature gradients induced by viscous heating are very pronounced local instabilities occur and the triggering of secondary flows is possible.

Summarizing previous results (see Costa & Macedonio (2003) and references therein), we know that, in steady state conditions for a fully developed Poiseuille or Couette flow, there is a critical value of a non-dimensional “shear-stress” parameter $\mathcal{G} = \mathcal{G}_{crit}$, for which when $\mathcal{G} > \mathcal{G}_{crit}$ the system does not admit solution, while when $\mathcal{G} < \mathcal{G}_{crit}$, the system has two solutions, one of which (the solution with greater temperature) may be unstable.

For finite length tubes, Costa & Macedonio (2003) have shown that these processes are controlled principally by the Peclet number Pe , the Nahme number Na (also called Brinkman number), and the non-dimensional flow rate q :

$$Pe = \rho c_p UH/k; \quad Na_0 = \mu_0 U^2 \beta / k; \quad q = \mu_0 Q / (\rho g H^3) \quad (1.1)$$

with ρ density, c_p specific heat, U mean velocity, H tube radius, k thermal conductivity, μ_0 reference viscosity (Na_0 is based on this value), β rheological parameter (see eq.2.1) and Q flow rate per unit length ($Q = UH$).

When viscous heating is important, starting with uniform temperature and parabolic velocity profile at the inlet, the flow evolves gradually to a plug-like velocity profile with two symmetric peaks in the temperature distribution. The most important are viscous dissipation effects: the more pronounced the temperature peaks, the lower the length scale for the development of the plug flow (Costa & Macedonio 2003; Ockendon 1979).

Because of the typically low thermal conductivity of these liquids (e.g. silicate melts), the temperature field shows a strong radial gradient. Due to the strong coupling between viscosity and temperature, the thermal instability generated by viscous heating may trigger an instability in the velocity field that cannot be predicted by a simple isothermal newtonian models. Flows with layers of different viscosity were investigated in the past, for their practical interest, and it is known that they are not always stable (Yih 1967; Craik 1969; Renardy & Joseph 1985; Renardy 1987). The instabilities are generated by

the viscosity contrasts, and are similar to the Kelvin-Helmholtz instabilities triggered by density gradients. The stability of the plane Couette flow was recently re-examined by Yueh & Weng (1996), who improve the results previously obtained by Sukanek *et al.* (1973). The flow shows two different instability modes: the former arises in the non-viscous limit, and the latter is due to the viscosity stratification (Yueh & Weng 1996). For this last instability mode, it was demonstrated that the critical Reynolds number, above which the flow becomes turbulent, decreases with the increase of the Nahme number, that is with the viscous heating. This behaviour has been confirmed by recent experiments (White & Muller 2000). In these experiments, the authors use a temperature-dependent fluid (glycerin) and a Taylor-Couette device which allows the tracking of vortex by a laser particle tracer. Results clearly show that above a critical Nahme number an instability appears at a Reynolds number one order of magnitude lower than the corresponding Reynolds number predicted for isothermal flow.

In this study, the fully two-dimensional transport equations for mass, momentum and energy are numerically solved. In particular we focus our attention on the velocity and temperature field evolution in the case that viscous heating effects completely control physical processes of the flow. We restrict our investigations to the physical regime with low Reynolds number $Re < O(10^2)$, high Nahme number $Na \gg 1$, high Peclet number $Pe \gg 1$ and high Prandtl number $Pr \gg 1$.

2. Model description

We consider an incompressible homogeneous fluid with a constant density, specific heat and thermal conductivity. The fluid viscosity μ is temperature-dependent and the exponential (Nahme's) law is assumed:

$$\mu = \mu_0 \exp[-\beta(T - T_0)] \quad (2.1)$$

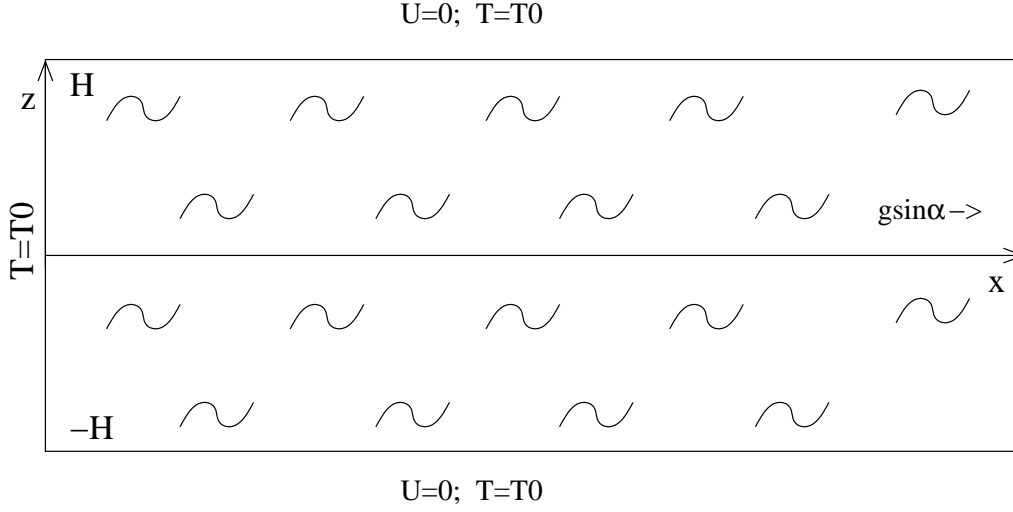


FIGURE 1. Sketch of the studied system.

where T is temperature β a rheological factor and μ_0 is the viscosity value at the reference temperature T_0 . We investigate the two-dimensional flow in a slab between two parallel boundaries of length L separated by a distance $2H$ (with $H/L \ll 1$) and inclined at an angle α with respect to the horizontal (see Figure 1). In these hypotheses, fluid dynamics in the tube are described by the following transport equations expressed in dimensionless form:

$$\frac{\partial u_i}{\partial \xi_i} = 0 \quad (2.2)$$

$$\frac{\partial u_i}{\partial \tau} + v_j \frac{\partial v_i}{\partial \xi_j} = \frac{1}{Fr_c} g_i^* - \frac{\partial \tilde{p}}{\partial \xi_i} + \frac{1}{Re_c} \frac{\partial}{\partial \xi_j} \left[e^{-\theta} \left(\frac{\partial v_i}{\partial \xi_j} + \frac{\partial v_j}{\partial \xi_i} \right) \right] \quad (2.3)$$

$$\frac{\partial \theta}{\partial \tau} + v_j \frac{\partial \theta}{\partial \xi_j} = \frac{1}{Pe_c} \frac{\partial}{\partial \xi_j} \frac{\partial}{\partial \xi_j} \theta + \frac{Na_c}{Pe_c} \frac{e^{-\theta}}{2} \left(\frac{\partial v_i}{\partial \xi_j} + \frac{\partial v_j}{\partial \xi_i} \right)^2 \quad (2.4)$$

where $\tau = tU_c/H$ is the dimensionless time, $(\xi_1, \xi_2) = (x/H, z/H)$ are the longitudinal and transversal dimensionless coordinates, $(u_1, u_2) = (v_x/U_c, v_y/U_c)$ represent the dimensionless field velocity (scaled of a characteristic velocity U_c), $(g_1^*, g_2^*) = (g_x/g, g_y/g)$ the dimensionless gravitational field (g is the gravitational acceleration), $\theta = \beta(T - T_0)$ the dimensionless temperature and $p^* = p/(\rho U_c^2)$ is the dimensionless pressure (index Einstein's convention was used). The meaning of the usual characteristic dimensionless

Name	Symbol	Definition	Value	Symbol	Definition	Value
Reynolds number	Re_c	$\rho U_c H / \mu_0$	4.5	Re	$\rho U H / \bar{\mu}$	120
Nahme number	Na_c	$\beta \mu_0 U_c^2 / k$	14.4	Na	$\beta \bar{\mu} U^2 / k$	2400
Peclet number	Pe_c	$\rho c_p U_c H / k$	450	Pe	$\rho c_p U H / k$	7400
Froude number	Fr_c	$U_c^2 / (gH)$	0.3	Fr	$U^2 / (gH)$	84
Prandtl number	Pr_c	$\mu_0 c_p / k$	100	Pr	$\bar{\mu} c_p / k$	62
Batchelor number	Ba_c	$H / L_B(U_c)$	4.9	Ba	H / L_B	45.5
Aspect ratio	γ	H / L	3/100	γ	H / L	3/100

TABLE 1. Typical dimensionless numbers. The calculated values on the left are based on the mean Poiseuille velocity $U_P = \rho g H^2 \sin \alpha / (3\mu_0)$. The calculated values on the right are instead based the mean velocity U and mean viscosity $\bar{\mu}$.

numbers is reported in table 1.

The last term in the equation (2.4) represents the heat generation by viscous dissipation.

Since we have considered a symmetric geometry and symmetric boundary conditions, we investigate only half channel ($0 \leq \xi_2 \leq 1$). As boundary conditions we considere no-slip velocity and isothermal temperature at walls: $u_i = 0$ and $\theta = 0$ at $\xi_2 = 0$. At the inlet we assume free flow conditions and the fluid temperature to be the same as the wall temperature: $\theta_{in} = 0$. As initial conditions we set zero dimensionless velocity and temperature.

We are interested to solve the problem of a free viscous flow in an inclined slab-tube (see Figure 1) in the case of low Reynolds number regime. In fact, considering the geometry of Figure 1 and the isothermal case without viscous heating effects, the Navier-Stokes equations of a viscous liquid in the gravitational field admit a simple solution

(Landau & Lifchitz 1994):

$$\mu_0 \frac{d^2 V}{dz^2} + \rho g \sin \alpha = 0 \quad \frac{dp}{dz} + \rho g \cos \alpha = 0 \quad (2.5)$$

In this case, the mean velocity is $U_P = gH^2 \sin \alpha / (3\nu_0)$ with $\nu_0 = \mu_0 / \rho$. From this point onwards we choose this velocity as the characteristic reference velocity: $U_c = U_P$ (in table 1 $U_P = 0.3\text{m/s}$ was set).

The parameter values reported in table 1 are chosen in order that the computational requests are not completely restrictive and the system can be considered belong to the regime with $Re < \mathcal{O}(10^2)$, $Na \gg 1$, $Pe \gg 1$ and $Pr \gg 1$. In fact, our aim is to fully simulate the flow field evolution when viscous heating effects are very important. To do this, there is a need to solve all the involved length scales of the problem: from the integral length H up to the dissipative scale. In the ordinary direct numerical simulation the dissipative scale is few times the Kolmogorov length:

$$L_K = \left(\frac{\nu^3}{\epsilon} \right)^{1/4} \quad (2.6)$$

where ϵ is the energy dissipation rate (Smyth & Moum 2000*a*; Moin & Mahesh 1998). Since $H/L_K \sim Re^{3/4}$ and our integral-scale Reynolds number $Re = HU/\nu$ is small, this condition does not appear very restrictive, but unfortunately when the Prandtl number is large, $Pr \gg 1$, as in our case, the dissipative scale is the Batchelor length (Smyth & Moum 2000*a*):

$$L_B = \frac{L_K}{\sqrt{Pr}}; \quad (2.7)$$

hence $H/L_B \sim Re^{3/4} Pr^{-1/2}$. When $L_K > L_B$ temperature fluctuations can occur at scales smaller than the velocity fluctuation scales (Smyth & Moum 2000*a,b*). Moreover, since turbulence tends to be isotropic a very fine horizontal resolution is required.

3. Solution method and numerical aspects

To solve equations (2.2)-(2.3)-(2.4), a fortran code based on the Finite Element Method was used. Isoparametric 8-node elements with linear piecewise approximation of the velocity and temperature fields were adopted. The velocity and the temperature fields are assumed continuous across the element boundaries, whereas the pressure field was approximated by constant functions inside each element, and discontinuous across the inter-element boundaries. This choice improves the stability of the numerical solution for incompressible fluids, according to the approach used by Brooks & Hughes (1982). Moreover, the Streamline Upwind Petrov-Galerkin method was adopted to reduce numerical instabilities at high Reynolds and/or Peclet numbers. Although the studied regime is characterized by low Reynolds number and we used a first-order upwind scheme, high-order-accurate schemes should be used (Rai & Moin 1991).

Equations 2.2-2.4 are solved using the Predictor/Multicorrector method as suggested by Brooks & Hughes (1982), with the addition of the enthalpy equation in a similar way as suggested by Heinrich & Yu (1988). The solution method is explicit in the velocity and temperature and implicit in the pressure, this last being computed through the solution of a Poisson equation.

Convergence of the algorithm is assured when the element Courant number Cr satisfies particular conditions depending on the element Reynolds and Peclet numbers. Typically, to assure the convergence, the element Courant number should satisfy the most restrictive among the following relations (Brooks & Hughes 1982):

$$Cr \leq 0.8, \quad \text{if } \alpha \geq 100,$$

$$Cr \leq \min(1, \alpha), \quad \text{if } \alpha < 100.$$

where $Cr = v\Delta t/\Delta x$, with v , Δt and Δx respectively element velocity, computational

time step and computational grid size, and α represents both the element Reynolds and Peclet numbers. Unfortunately, the above convergence criteria are very restrictive, forcing the choice of a very small time step to guarantee the convergence of the algorithm.

3.1. Numerical parameters evaluation

From a practical point of view, an estimation of L_B requires the mean velocity U and, since in our case the viscosity is variable, the mean kinematics viscosity $\bar{\nu}$. In fact, an evaluation ϵ is given by:

$$\epsilon = \frac{CU^3}{H} \quad (3.1)$$

where $C = 6.5 \cdot 10^{-4}$ (Smyth & Moum 2000a). From previous results (Costa & Macedonio 2003), we know that a viscosity decrease induced by local viscous heating near the tube walls can permit an increase of velocity. Obviously the steady mean velocity U is generally different with respect to the isothermal case where $U = U_P$. But the evaluation of L_B requires at least an estimation of the mean velocity U . To overcome this difficulty, we used $U = U_P$ as a guess value for obtaining a first estimation of L_B^0 that we used as a minimum grid size $\Delta\xi^{(0)}$ (or equal to the first L_B^0 -fraction that guarantees a numerical convergency). The use of this grid size gave a new value of U that was used to estimate again L_B^1 and therefore $\Delta\xi^{(1)}$. The process was repeated until the value of U appeared to reach to a convergency value. The grid dependence on the dimensionless mean velocity U/U_P is shown in figure 2.

The final dimensionless numbers and others parameters based on the mean velocity and mean viscosity are reported in table 1.

The computational grid was formed by an uniform horizontal grid size $\Delta x/H$ and three different increasing vertical grid sizes $\Delta z_1/H$, $\Delta z_2/H$ and $\Delta z_3/H$ (the finest is close to walls and largest is in correspondence to the channel center). The final grid size values at

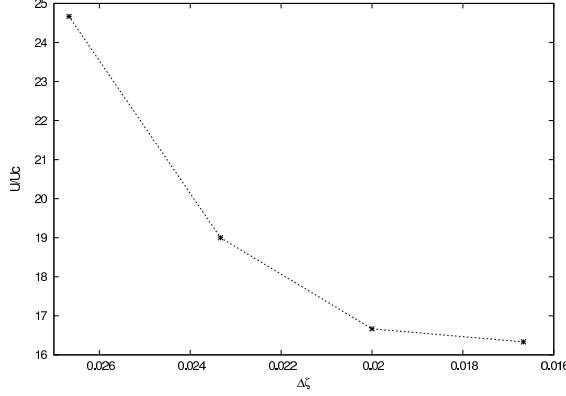


FIGURE 2. U -grid size dependence in the different simulations performed by decreasing the vertical grid size. Along the x -axis and y -axis the finest grid size and the mean velocity are respectively reported.

which the computational algorithm appears to converge are given from $\Delta x/L_B = 3.78$ ($\Delta x/H = 0.084$) and $\Delta z_i/L_B = 0.76; 1.36; 2.12$ ($\Delta z/H = 0.0167; 0.0299; 0.0466$). The finest grid size is set near the wall, where gradients change suddenly and the viscosity is very low.

4. Results and discussion

As the time increases the temperature starts to rise in the region near the outlet because of viscous heating. At $\tau = \tau_* \approx 40$ an instability is triggered in this region where the dimensionless temperature θ locally becomes greater than ≈ 5 (see figures 6). For $\tau > \tau_*$, as viscous heating effects become more important even in the more internal region, secondary flows appear to organize themselves into coherent structures as rotational flows. This kind of secondary flow looks like roller vortices which move from the region near the outlet towards the inlet (see figures 6 where the streamlines are shown). This is the behaviour of the entire velocity and temperature field.

If we look at the temporal profile evolution at a given distance (for example at $2/3$ of

the tube length), from figures 3, we can see that θ , starting with a flat profile, gradually increases near the wall forming a profile with a maximum at a short distance from the lower boundary. With increasing time this peak becomes more pronounced ($\theta_{max} \lesssim 6$) filling, at the steady state, a narrow shell of values at a shorter distance of the wall (see figure 3). As consequence the dimensionless viscosity profile $e^{-\theta}$, strongly decreases in correspondence to the temperature peak, reaching values very low with respect the initial values (see figure 3). The layer where the molecular viscosity is very small is immediately the colder layer adjacent to the wall and it corresponds to the region where the vortices appear (see figure 6). This region is controlled by an effective eddy viscosity instead of the molecular viscosity.

The modulus velocity profile U/U_c , starting with a parabolic profile, evolves toward a plug profile filling at the steady state, a narrow region of values with a plug velocity $\lesssim 18$ (see figure 4). Instead, at the steady state, the vertical dimensionless velocity profile is characterised by the filling of an onion shape region (see figure 4).

Concerning the mean values of temperature, viscosity and velocity profiles, from figures 5 we can see that the mean temperature rapidly increases (in an interval of $\tau \approx 20$), then decreases reaching a steady state weakly oscillating value around $\theta \approx 1$. As a consequence, the dimensionless viscosity, rapidly decreases then increases reaching a weakly oscillating steady state around 0.6. However the dimensionless mean velocity U/U_c reaches a steady state value in a longer time, assuming a value of about 16 only after $\tau \approx 150$. The mean values of temperature, viscosity and velocity summarized in table 1, show that the effects of viscous heating drastically change the flow properties. In fact the Reynolds number based on the real mean velocity and viscosity, Re , is more than twenty times greater than the corresponding Reynolds number for the isothermal case Re_c . The Nahme number Na is more than two orders of magnitude of Na_c .

From these results, it is evident that in the case of flows between two parallel planes, cylindrical secondary flows develop near the walls (for circular pipes we can infer that toroidal secondary flows can occur) without any unlimited increase in the temperature as predicted by simpler unidimensional models.

The obtained simulations could be used to parameterize the effective eddy viscosity that control these kind of flows in a simple way (e.g. using a Smagorinsky approach with a different constant), but obviously a larger amount of data are needed.

4.1. Validity and limits of the method

We have seen that when viscous heating is relevant, a special class of secondary flows can develop in fluids with temperature dependent viscosities even at low Reynolds numbers. This kind of “turbulence” is locally confined near the wall where there is a large unstable viscosity gradient and the viscosity is low.

The obtained results are valid in the limit of a two dimensional model based on the full solution of the Navier-Stokes equations but turbulence is generally three-dimensional even starting with an two-dimensional initial conditions. On the other hand, it is known that the growth of three-dimensional instabilities is suppressed by a strong anisotropy (Sommeria & Moreau 1982; Messadek & Moreau 2001). This anisotropy can be due to the presence of a magnetic field (Sommeria & Moreau 1982), a strong rotation and/or a density stratification (Lilly 1972; Hopfinger 1987; van Heijst 1993). A feature of 2D turbulence is that two-dimensional vortices can form coherent structures on large scale (van Heijst 1993).

In our case, the strong viscosity stratification induce by viscous heating produces a strong anisotropy that should imply the two-dimensional model we used is able to account for the essential physical properties of the real systems.

Finally, concerning the used numerical scheme we must stress its limits for this study:

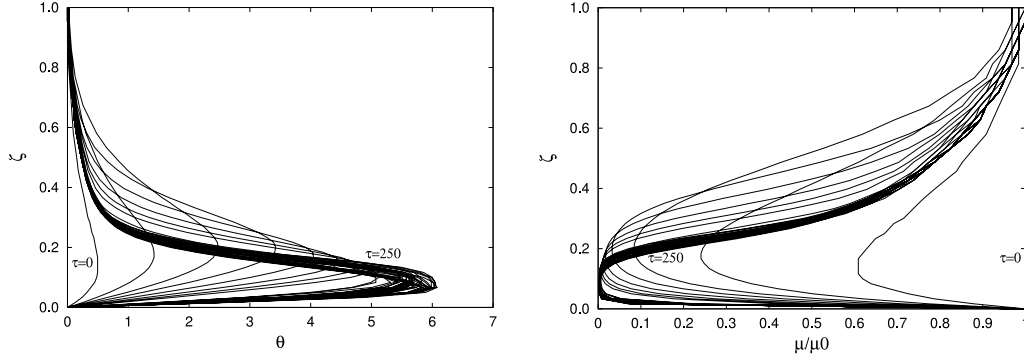


FIGURE 3. Temporal evolution from $\tau = 0$ to $\tau = 250$ of dimensionless temperature profile (on the left) and dimensionless viscosity profile (on the right), at $H\xi_1 = 2/3L$ distance from inlet.

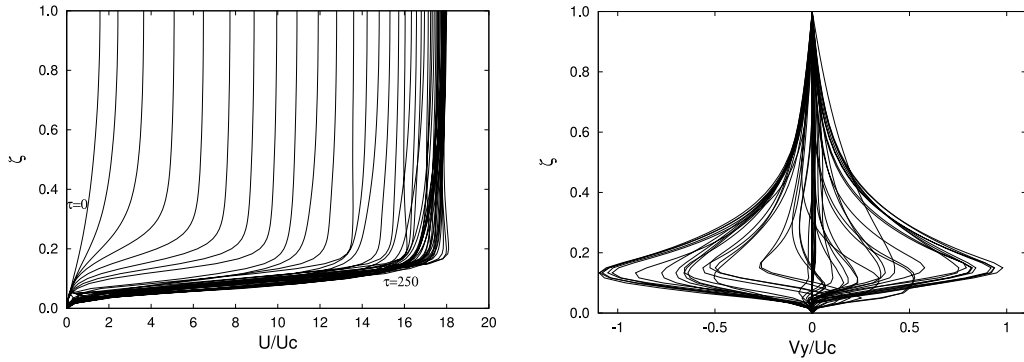


FIGURE 4. Temporal evolution from $\tau = 0$ to $\tau = 250$ of the dimensionless velocity modulus profile (on the left) and of the dimensionless transversal velocity profile (on the right), at $H\xi_1 = 2/3L$ distance from inlet.

the scheme has a first-order upwind and to be accurate needs very restrictive conditions and a large computational time. A more suitable scheme should be used to permit a more detailed study and to investigate the role of each control parameter.

In any case, we hope that this paper stimulates further more accurate studies on this intriguing topic, contributing to a more quantitative comprehension of this problem which has many practical implications, e.g in magma flows (see e.g. Costa & Macedonio (2003) and references therein).

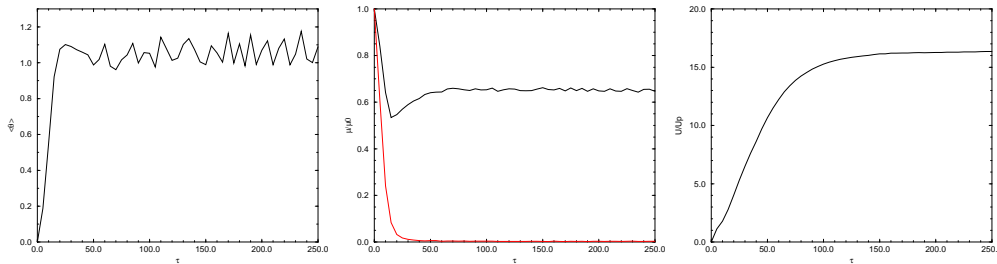


FIGURE 5. Temporal evolution from $\tau = 0$ to $\tau = 250$ of the dimensionless mean temperature (on the left), mean viscosity (in the centre) and mean velocity (on the right), at $H\xi_1 = 2/3L$ distance from inlet. In the figure in the centre the minimum dimensionless viscosity value is also reported (red line).

Conclusion

The thermo-fluid-dynamics of a fluid with strongly temperature-dependent viscosity in a regime with low Reynolds numbers, high Peclet and high Nahme numbers were investigated by direct numerical simulation.

Our results show that viscous heating can drastically change the flow features and fluid properties. The temperature rise due to the viscous heating and the strong coupling between viscosity and temperature can trigger an instability in the velocity field, which cannot be predicted by simple isothermal newtonian models. We showed as viscous heating can be responsible of triggering and sustaining of a particular class of secondary rotational flows which appear organized in coherent structures similar to roller vortices. We wish that our preliminary results can stimulate further more accurate studies on this intriguing topic, contributing to a more quantitative comprehension of this problem which has many practical implications for example in the dynamics of magma flows in conduits and lava flows in channels.

REFERENCES

BROOKS, A. & HUGHES, T. 1982 Streamline upwind/Petrov-Galerkin formulations for convec-

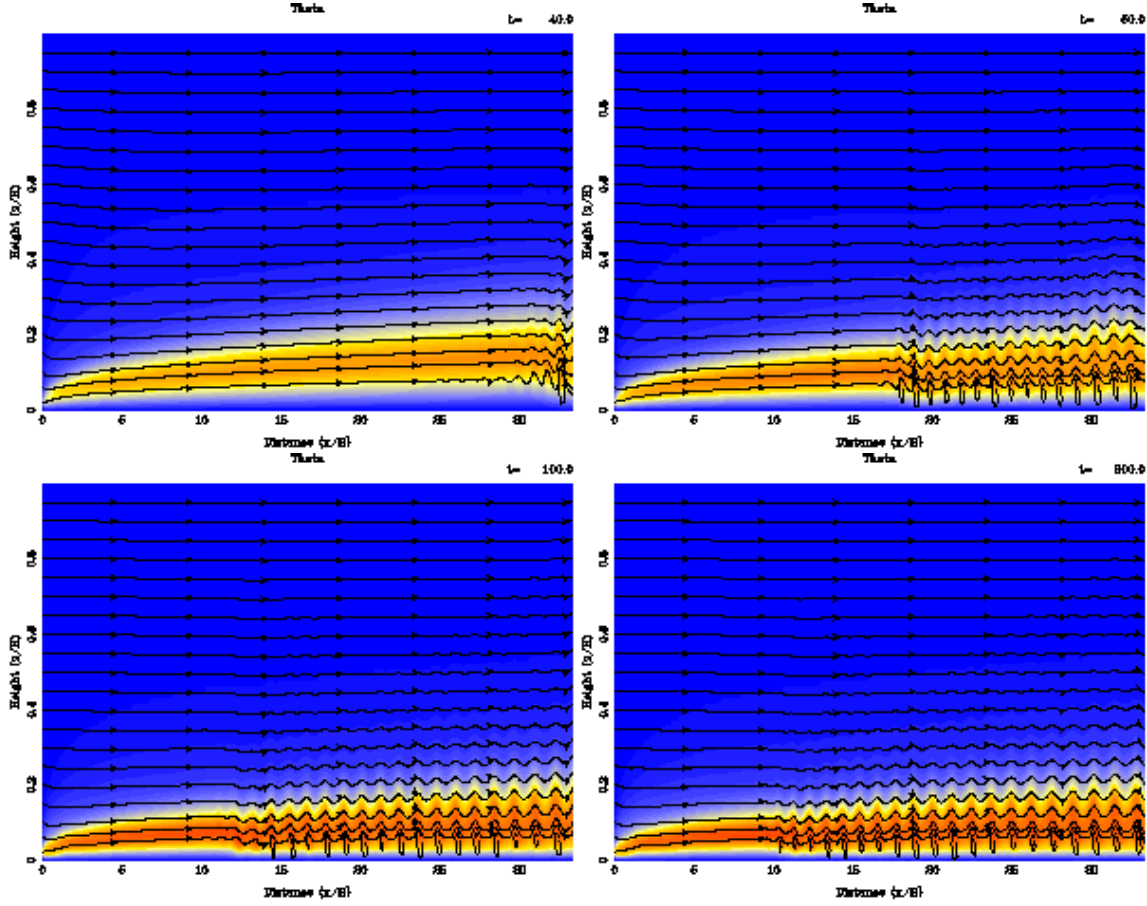


FIGURE 6. Evolution of the dimensionless flow fields. The figures show the simulated streamlines with the temperature field as background for different τ -values. The blue colour indicates the lowest dimensionless temperature ($\theta = 0$) and the darkest orange corresponds to the highest temperature ($\theta = 6$). The symbol t on the upper right corner indicates the dimensionless time τ . For visualization reasons the horizontal axis is contracted with respect to the vertical.

tion dominated flows with particular emphasis on the incompressible Navier-Stokes equations. *Comput. Methods Appl. Mech. Engrg.* **32**, 199–259.

COSTA, A. & MACEDONIO, G. 2003 Viscous heating in fluids with temperature-dependent viscosity: implications for magma flows. *Nonlinear Proc. Geophys.* **10** (6), 545–555.

CRAIK, A. 1969 The stability of plane Couette flow with viscosity stratification. *J. Fluid Mech.* **36** (2), 687–693.

VAN HEIJST, G. 1993 Self-organization of two-dimensional flows. *Nederlands Tijdschrift voor Naturkunde* **59**, 321–325.

- HEINRICH, J. & YU, C. 1988 Finite elements of buoyancy-driven flows with emphasis on natural convection in horizontal circular cylinder. *Comput. Methods Appl. Mech. Engrg.* **69**, 1–27.
- HOPFINGER, E. 1987 Turbulence in stratified fluids: a review. *Phys. Fluids* **92**, 5287–5303.
- LANDAU, L. & LIFCHITZ, E. 1994 *Physique Theorique - Mecanique des fluides*, 3rd edn. Moscow: MIR.
- LILLY, D. 1972 Numerical simulation of two-dimensional turbulence. *Phys. Fluids* **Supplement II**, 240–249.
- MESSADEK, K. & MOREAU, R. 2001 Quelques resultats sur la turbulence MHD quasi-2D. In *Proc. XV Congrès Francais de Mecanique*. Nancy.
- MOIN, P. & MAHESH, K. 1998 DNS: A tool in turbulence research. *Annu. Rev. Fluid Mech.* **30**, 539–578.
- OCKENDON, H. 1979 Channel flow with temperature-dependent viscosity and internal viscous dissipation. *J. Fluid Mech.* **93** (4), 737–746.
- PEARSON, J. 1977 Variable-viscosity flows in channels with high heat generation. *J. Fluid Mech.* **83** (1), 191–206.
- RAI, M. & MOIN, P. 1991 Direct simulations of turbulent flow using finite-difference schemes. *J. Comp. Phys.* **96**, 15–33.
- RENARDY, Y. 1987 Viscosity and density stratification in vertical Poiseuille flow. *Phys. Fluids* **30** (6), 1638–1648.
- RENARDY, Y. & JOSEPH, D. 1985 Couette flow of two fluids between concentric cylinders. *J. Fluid Mech.* **150**, 381–394.
- SMYTH, W. & MOUM, J. 2000*a* Length scales of turbulence in stably stratified mixing layers. *Phys. Fluids* **12**, 1327–1342.
- SMYTH, W. & MOUM, J. 2000*b* Ocean turbulence. In *Encyclopedia of Ocean Sciences*. Academic Press.
- SOMMERIA, J. & MOREAU, R. 1982 Why, how and when MHD turbulence becomes two-dimensional? *J. Fluid Mech.* **118**, 507–518.
- SUKANEK, P., GOLDSTEIN, C. & LAURENCE, R. 1973 The stability of plane Couette flow with viscous heating. *J. Fluid Mech.* **57** (part 4), 651–670.

- WHITE, J. & MULLER, S. 2000 Viscous heating and the stability of newtonian and viscoelastic Taylor-Couette flows. *Phys. Rev. Lett.* **84** (22), 5130–5133.
- YIH, C. 1967 Instability due to viscosity stratification. *J. Fluid Mech.* **27** (2), 337–352.
- YUEH, C. & WENG, C. 1996 Linear stability analysis of plane Couette flow with viscous heating. *Phys. Fluids* **8** (7), 1802–1813.